

This is the accepted manuscript made available via CHORUS. The article has been published as:

Symmetrical interfacial reconstruction and magnetism in
 $\text{La}_{0.7}\text{Ca}_{0.3}\text{MnO}_3/\text{YBa}_2\text{Cu}_3\text{O}_7/\text{La}_{0.7}$
 $\text{Ca}_{0.3}\text{MnO}_3$ heterostructures

C. Visani, J. Tornos, N. M. Nemes, M. Rocci, C. Leon, J. Santamaria, S. G. E. te Velthuis, Yaohua Liu, A. Hoffmann, J. W. Freeland, M. Garcia-Hernandez, M. R. Fitzsimmons, B. J. Kirby, M. Varela, and S. J. Pennycook

Phys. Rev. B **84**, 060405 — Published 23 August 2011

DOI: [10.1103/PhysRevB.84.060405](https://doi.org/10.1103/PhysRevB.84.060405)

**Symmetrical interfacial reconstruction and magnetism in
 $\text{La}_{0.7}\text{Ca}_{0.3}\text{MnO}_3/\text{YBa}_2\text{Cu}_3\text{O}_7/\text{La}_{0.7}\text{Ca}_{0.3}\text{MnO}_3$ heterostructures**

C. Visani, J. Tornos, N. M. Nemes, M. Rocci, C. Leon, J. Santamaria

GFMC. Dpto. Física Aplicada III, Universidad Complutense de Madrid. Campus Moncloa, 28040 Madrid. Spain

S. G. E. te Velthuis, Yaohua Liu, A. Hoffmann.

Materials Science Division, Argonne National Laboratory, Argonne, Illinois 60439, USA

J. W. Freeland

Advanced Photon Source, Argonne National Laboratory, Argonne, Illinois 60439, USA

M. Garcia-Hernandez

Instituto de Ciencia de Materiales de Madrid. Consejo Superior de Investigaciones Científicas. 28049 Cantoblanco Spain

M.R. Fitzsimmons, B.J. Kirby*

Los Alamos National Laboratory, Los Alamos, New Mexico 87545, USA

M. Varela, S. J. Pennycook

Materials Science and Technology Division, Oak Ridge National Laboratory, Oak Ridge, Tennessee 37831-6071, USA

ABSTRACT

We have analyzed the interface structure and composition of $\text{La}_{0.7}\text{Ca}_{0.3}\text{MnO}_3/\text{YBa}_2\text{Cu}_3\text{O}_7/\text{La}_{0.7}\text{Ca}_{0.3}\text{MnO}_3$ trilayers by combined polarized neutron reflectometry, aberration corrected microscopy and atomic column resolution electron energy loss spectroscopy (STEM- EELS) and x-ray absorption with polarization analysis. We find the same stacking sequence at *both* top and bottom cuprate interfaces.

X-ray magnetic circular dichroism experiments show that *both* cuprate interfaces are magnetic with a magnetic moment induced in Cu atoms as expected from symmetric Mn-O-Cu superexchange paths. These results supply a solid footing for the applicability of recent theories explaining the interplay between magnetism and superconductivity in this system in terms of the induced Cu spin polarization at both interfaces [J. Salafranca and S. Okamoto, Phys. Rev. Lett. **105**, 256804 (2010)].

In recent years there has been a surge of interest on interplay between ferromagnetism and superconductivity in artificial thin film hybrids [1,2]. This interplay originates from the ferromagnet (F) / superconductor (S) proximity effect by which Cooper pairs penetrate into the ferromagnet, directly experiencing the exchange interaction [3-11]. As a result the effect is short range, and the relevant length-scale becomes shorter with increasing spin polarization of the ferromagnet, and should vanish in the limit of full spin polarization, *i.e.*, a half metal. Superconductivity is also suppressed in the superconducting layer over length scales given by the superconducting coherence length. Recent studies on $\text{La}_{0.7}\text{Ca}_{0.3}\text{MnO}_3$ (LCMO) / $\text{YBa}_2\text{Cu}_3\text{O}_7$ (YBCO) epitaxial heterostructures demonstrate superconductivity suppression of the superconducting critical temperature over length scales much larger (1-2 orders of magnitude) than the coherence length of the cuprate [12,13]. This can be hardly explained in terms of a (singlet) proximity effect given the high spin polarization of the manganite and the sub-nanometer coherence length of the cuprate. Other explanations in terms of (self) diffusion of spin polarized quasiparticles [14] or induction of a triplet superconductivity component [15] also do not account for the long length scale of the superconductivity suppression in the cuprate. The strong electronic and orbital reconstruction occurring at this interface gives rise to an induced negative spin polarization of the cuprate interface as found in [16, 17] and very recently confirmed by [18]. This may arise due to a canting of the antiferromagnetic Cu sublattice induced by the interfacial (antiferromagnetic) Mn-O-Cu superexchange interaction. Recent theoretical calculations [19] have shown that Cu spin polarization, which does not originate from a proximity effect but from orbital reconstruction, accounts semi-quantitatively for most experimental observations. Furthermore, this mechanism also explains the inverse spin switch behaviour observed in F/S/F structures where superconductivity is enhanced when the F layer magnetizations are parallel [20]. The balance between applied magnetic field and (the exponential tail of the) effective field due to the interfacial antiferromagnetic superexchange interaction cancel out when the layers are parallel giving rise to a small shift of the resistance curve towards higher transition temperatures.

The applicability of the orbital reconstruction mechanism depends critically on the existence of a superexchange path linking Mn atoms and planar Cu atoms in the

cuprate at both interfaces. This implies certain symmetry in the orbital and electronic reconstruction at both interfaces, a situation which can not be taken for granted in epitaxial layers. In fact, it has been recently pointed out that in superlattices (A-B-A-B-A...) mirror interfaces (A-B and B-A) need not be identical [21, 22]. While preliminary results of interface analysis of LCMO/YBCO samples grown by sputter deposition (similar to those reported in this work) suggest symmetric interfaces, recent reports of aberration corrected STEM on YBCO/LCMO interfaces grown by PLD indicate that top and bottom interfaces of a manganite layers sandwiched between YBCO are different [23]. The dichroism experiments where the Cu moment was first reported [16, 17] supplied information only about the top-most interface due to the high surface sensitivity of the total electron yield (TEY) method used. The question then arises if there is Cu magnetism at both interfaces and how it is affected by any possible asymmetry of the interfaces. In this paper we address this question by examining the interface reconstruction in trilayers $\text{La}_{0.7}\text{Ca}_{0.3}\text{MnO}_3$ (LCMO) / $\text{YBa}_2\text{Cu}_3\text{O}_7$ (YBCO) / $\text{La}_{0.7}\text{Ca}_{0.3}\text{MnO}_3$ (LCMO) with x-ray magnetic circular dichroism (XMCD) experiments. The small, 7 nm thick, YBCO thickness together with an x-ray resonant magnetic scattering detection method of the Cu dichroic signal enables us to obtain information about the Cu magnetic state at both interfaces. The respective magnetism could be separated due to the different coercivities of top and bottom LCMO layers.

We grew F/S/F trilayers with fixed 15-nm thick top and bottom LCMO layers while the YBCO thickness ranges between 7 and 47 nm. This manuscript focuses on the 7nm YBCO thick samples although results of thicker samples will be commented. This small thickness of the YBCO allows obtaining magnetic information from both interfaces. The samples were grown by sputter deposition in pure oxygen pressure [12, 13] on (100) SrTiO_3 substrates with mixed termination. Sample structure was also probed by scanning transmission electron microscopy (STEM). Z-contrast images were obtained in a Nion UltraSTEM operated at 100 kV and equipped with a 5th order corrector and a Gatan Enfina spectrometer to allow simultaneous imaging and electron energy loss spectroscopy (EELS). Random noise in the EELS spectrum images was removed using Principal Component Analysis [24]. We performed XMCD measurements at the Advanced Photon Source (Argonne National Laboratory) at beamline 4-ID-C. We performed Polarized Neutron Reflectivity (PNR) experiments using the ASTERIX reflectometer, and Cu $K\alpha$ X-ray reflectivity (XR) at the Lujan

Neutron Scattering Center (Los Alamos National Laboratory). Reflectivity data was fit using the Co-Refine program [25] which applies the Parratt formalism for calculating the reflectivity from models for the depth-dependent X-ray and/or Neutron scattering length density (SLD) profiles [26].

The combined refinement (i.e. fitting) of the XR and PNR data, the latter collected in a magnetically saturated state (at $H = 5.55$ kOe), provides surface-averaged chemical (i.e. nuclear) and magnetic depth profiles of the sample [25, 27], shown in Fig 1 for a trilayer with 7 nm thick YBCO at a temperature of 9.5K. The sample is superconducting with a zero resistance T_c of 30 K. Samples with thicker YBCO showed weaker superconductivity suppression until for samples thicker than 15 nm bulk T_c is recovered [12], ruling out oxygen deficiency as the origin of T_c reduction [28]. The magnetic SLD is directly proportional to the magnetization [25, 27]. The X-ray and neutron nuclear depth profiles show that the roughnesses of the top LCMO layer are larger than those of the bottom LCMO layer and that the average magnetization is reduced. An additional suppression of the top LCMO layer magnetization is observed at the interface with YBCO, which has previously been interpreted to result from electron transfer from the manganite into the cuprate [29, 30]. The magnetization of the bottom LCMO layer corresponds to that of bulk LCMO. The depth resolution and sensitivity of the PNR experiments done was not sufficient to resolve the moment on the interfacial Cu of the YBCO layer.

By tuning the X-ray circular polarization to the resonance energy of a specific electronic transition, one can obtain information on the chemical and magnetic state of a particular element. Soft X-rays in the energy range of Mn and Cu L-absorption edges were used to obtain element specific dichroic spectra where the magnetic signal is given by the difference between the right and left circularly polarized signals. In Fig. 2 we show x-ray resonant magnetic scattering (XRMS) and TEY XMCD data as a function of the photon energy taken at the Mn and Cu L_3 -absorption edge for the same trilayer of the XR and PNR experiments. A field of $H = -500$ Oe was applied in the plane of the sample along the [110] crystallographic direction at a temperature of 30 K. The induced Cu moment observed at the Cu L_3 -edge has been demonstrated to originate from canted Cu spins of the interfacial CuO_2 layer in the YBCO, coupled antiferromagnetically with the nearest Mn moments of the LCMO [16, 17]. In contrast to absorption (TEY) spectroscopy, the reflectivity signal is also sensitive to dispersive parameters and

necessitates modelling to extract absolute value for the magnetic moment of each LCMO layer. Regardless, since the x-ray resonant magnetic scattering (XRMS) signal is proportional to the magnetization, the signal was monitored while sweeping the magnetic field to record a hysteresis loop as shown in the bottom panel of Fig. 3 [31]. It should be noted though, that the ratio of the steps in a multilayered sample can deviate from the expected values due to changes in the interference conditions with changes in the magnetic configuration. Sweeping a magnetic field has a strong influence on the secondary electrons collected to yield the TEY signal. To get an adequate reflectivity signal from the Cu edge we summed over a large number of subsequent hysteresis loops as measured with XRMS (up to 80) after setting the energy to the peak position observed in the TEY mode: at 645.5 eV for the Mn L-edge and at 932.5 eV for the Cu L-edge with the beam oriented parallel to the external field and making an angle of 10 degrees with the sample surface to ensure deep penetration.

We measured two hysteresis loops: with the field applied along [100] and [110] axes. The hysteresis loops taken at the Mn L₃-edge highlight the different coercivities of both manganite layers. The PNR measurements (Fig. 1) indicate that the bottom LCMO layer switches first, as only that magnetization is found to be positive at H = 186 Oe and 335 Oe, fields intermediate between the two coercivities, following negative saturation. This probably results from a difference in the strain state, since during the growth of the YBCO layer the first LCMO layer will be fully strained while the top LCMO layer is (partially) strain relaxed. The larger coercivity and remanent magnetization along the [110] direction is indicative of magnetic fields aligned with the easy axis [32]. Figure 3(b) shows the hysteretic behavior of the Cu magnetic moments through XMRS hysteresis loops. Cu and Mn loops display similar shape and coercivities: it becomes clear that the Cu moments switch follow closely the switching of the Mn moments. This is because the Cu magnetism results from the antiferromagnetic coupling to the interfacial Mn. Moreover, the fact that the magnetic response of Cu and Mn are similar indicates that the Cu at both interfaces is responding in the same proportion to Mn magnetic moments. The Cu loops display the two coercive fields confirming that both interfaces are magnetic as also indicated by the fits to the PNR data. Moreover, the presence of Cu magnetism at both interfaces suggests that there are similar Mn-O-Cu superexchange paths linking interfacial Mn and planar (CuO₂) Cu atoms. Similar

samples with thicker YBCO (12 nm and higher) showed only the Cu signal due to the top interface.

We have examined the interface structure and composition in our samples by aberration corrected STEM using a similar sample to that of the dichroism experiment. Fig. 4 displays a high magnification Z contrast STEM image of a LCMO (top) / YBCO (middle) / LCMO (bottom) trilayer. The layers show good epitaxial properties and coherent growth. EELS spectrum images were acquired to investigate the interface structure. Figure 4(a) shows a high resolution image of a sample with the same thickness of the individual layers. The darker planes corresponding to CuO chains of YBCO are missing at both interfaces. Elemental maps corresponding to the O K Mn L_{2,3}, Ba M_{4,5}, and La M_{4,5} edges are shown in Figs. 4(b)-(e), respectively. The atomic lattices of all these elements are clearly resolved. Interestingly, the LCMO layer looks chemically wider on the Mn image than on the La map. These maps indicate a (BaO) atomic plane termination for both the top and bottom interfaces of the cuprate and MnO₂ of the manganite at both interfaces. These results are consistent with *both* interfaces displaying the same termination with a plane sequence YBCO- BaO- CuO₂- Y - CuO₂- BaO- MnO₂- (La,Ca O)- LCMO as reported previously by some of us in similar samples [30]. This observation is more evident when the compositional maps are coloured and overlaid as done in Fig. 4(f): a blue BaO plane faces a red MnO₂ plane for both the top and bottom interfaces. This is at variance with the interface structure of PLD deposited samples reported recently [23] which display the plane sequence YBCO- BaO- CuO₂- (La,Ca O)- MnO₂- LCMO (top) and LCMO- (La,Ca O)- MnO₂ - BaO - CuO- BaO- CuO₂ -Y- CuO₂ - YBCO (bottom). Notice that in the PLD samples at the bottom interface the Mn atoms are coordinated to chain Cu atoms (instead to plane Cu). I.e., there is not a direct Mn- O- Cu superexchange path to planar Cu atoms.

In summary, we have found a symmetric interface reconstruction at both cuprate interfaces in LCMO/YBCO/LCMO structures. STEM- EELS analysis shows that the compositions of both interfaces are similar. This result contrasts with recent reports on PLD deposited samples showing asymmetric interface structure and evidences that interface reconstruction may depend on the growth technique in a way determined by temperature and oxygen pressure. This indicates that in our high oxygen pressure (3 mbar) and high temperature (900°C) growth process thermodynamics may play a more

important role than reaction kinetics. XMCD reflectivity hysteresis loops evidence that there is a spin polarization induced at (both) interfacial Cu atoms. The finding of Cu magnetism at both interfaces provide a firm footing for the applicability of recent models that explain the inverse spin switch behaviour of these trilayers in terms of the cancellation of the magnetic field associated with induced Cu moments by the applied field.

Acknowledgements

Work at UCM supported by Spanish MICINN Grant MAT 2008 06517, Consolider Ingenio CSD2009-00013 (IMAGINE), CAM S2009-MAT 1756 (PHAMA) and the European Research Council Starting Investigator Award, grant #239739 STEMOX. Argonne National Laboratory's work was supported by the U.S. Department of Energy, Office of Science, under contract No. DE-AC02-06CH11357. This work has benefited from the use of the Lujan Neutron Scattering Center at LANSCE, which is funded the Department of Energy's Office of Basic Energy Sciences. Los Alamos National Laboratory is operated by Los Alamos National Security LLC under DOE through Contract No. DE-AC52-06NA25396. Work at ORNL (MV, SJP) was supported by the Office of Science, Materials Sciences and Engineering Division of the US Department of Energy.

References

* Present address: National Institute of Standards and Technology, Gaithersburg, MD 20899.

- [1] A. I. Buzdin, *Rev. Mod. Phys.* **77**, 935 (2005).
- [2] F. S. Bergeret, A. F. Volkov, and K. B. Efetov, *Rev. Mod. Phys.* **77**, 1321 (2005)
- [3] J. Y. Gu *et al.* *Phys. Rev. Lett.* **89**, 267001 (2002)
- [4] A. Potenza and C. H. Marrows, *Phys. Rev. B* **71** 180503(R) (2005)
- [5] R. Steiner and P. Ziemann, *Phys. Rev. B* **74**, 094504 (2006)
- [6] I. C. Moraru, W. P. Pratt Jr and N. O. Birge *Phys. Rev. Lett.* **96**, 037004 (2006)
- [7] A. Yu. Rusanov, *et al.* *Phys. Rev. Lett.* **93**, 057002 (2004)
- [8] A. Singh, C. Sürgers, and H. v. Löhneysen, *Phys. Rev. B* **75**, 024513 (2007)
- [9] D. Stamopoulos, E. Manios, and M. Pissas, *Supercond. Sci. Technol.* **20** 1205 (2007)
- [10] Guo-Xing Miao, Ana V. Ramos, and Jagadeesh S. Moodera, *Phys. Rev. Lett* **101**, 137001 (2008)
- [11] J. Zhu, X. Cheng, C. Boone, I. N. Krivorotov, *Phys. Rev. Lett.* **V103** 027004 (2009)
- [12] Z. Sefrioui *et al.* *Phys. Rev. B* **67**, 214511 (2003)

- [13] V. Peña, Z. Sefrioui, M. Varela, D. Arias, C. Leon, J. L. Martinez, S. J. Pennycook and J. Santamaria, *Phys Rev. B.* **69**, 224502 (2004).
- [14] S. Soltan, J. Albrecht, and H. U. Habermeier, *Phys. Rev. B* **70**, 144517 (2004).
- [15] T. Hu, H. Xiao, C. Visani, Z. Sefrioui, J. Santamaria, C. Almasan, *Phys. Rev. B* **80**, R060506 (2009)
- [16] J. Chakhalian *et al.* *Nat. Phys.* **2**, 244 (2006)
- [17] J. Chakhalian *et al.* *Science.* **318**, 1114 (2007).
- [18] R. Werner, C. Raisch, A. Ruosi, B. A. Davidson, P. Nagel, M. Merz, S. Schuppler, M. Glaser, J. Fujii, T. Chassé, R. Kleiner, and D. Koelle, *Phys. Rev. B* **82**, 224509 (2010)
- [19] J. Salafranca and S. Okamoto, *Phys. Rev. Lett.* **105**, 256804 (2010)
- [20] V. Peña *et al.* *Phys. Rev. Lett.* **94**, 057002 (2005)
- [21] L. Koukoutis, D. A. Muller, Y. Hotta, and H. Y. Hwang, *Appl. Phys. Lett.* **91**, 1631010 (2007)
- [22] S. J. May, A. B. Shah, S. G. E. te Velthuis, M. R. Fitzsimmons, J. M. Zuo, X. Zhai, J. N. Eckstein, S. D. Bader, and A. Bhattacharya. *Phys. Rev. B* **77**, 174409 (2008).
- [23] Z. L. Zhang, U. Kaiser, S. Soltan, H. –U. Habermeier and B. Keimer *Appl. Phys. Lett.* **95**, 242505 (2009)
- [24] M. Bosman, M. Watanabe, D. T. L. Alexander, V. J. Keast. *Ultramicroscopy* **2006**, 106, 1024
- [25] M. R. Fitzsimmons and C. F. Majkrzak, *Modern Techniques for Characterizing Magnetic Materials*, edited by Y. Zhu, Springer, New York, 2005, pp. 107–155, Chap. 3.
- [26] L.G. Parratt, *Phys. Rev.* **95**, 359 (1954)
- [27] G.P. Felcher, R.O. Hilleke, R.K. Crawford, J. Haumann, R. Kleb, and G. Ostrowski, *Rev. Sci. Instrum.* **58**, 609 (1987)
- [28] Z. Sefrioui, D. Arias, M. Varela, J. E. Villegas, M. A. Lopez de la Torre, C. Leon, G. Loos and J. Santamaria, *Phys. Rev. B.* **60**, 15423 (1999).
- [29] A. Hoffmann *et al.* *Phys. Rev. B* **72**, 140407(R) (2005)
- [30] M. Varela *et al.* *Solid State Electronics*, **47**, 2245 (2003)
- [31] J.W. Freeland *et al.* *J. Phys. Cond. Mat.* **19**, 315210 (2007)
- [32] N. M. Nemes *et al.*, *Phys. Rev. B.* **81**, 094512 (2010).

Figure captions

Figure 1. (Color online) a) Non-spin flip reflectivity of neutrons polarized parallel to the applied field (R^{++}) and antiparallel (R^{--}) to the applied field, measured at 9.5K at the indicated fields after zero-field cooling. Spin-flip reflectivities, not shown, were zero indicating the magnetizations were co-linear to the applied fields. Black lines are fits to the data. Reflectivities for $H = 335$ Oe are reduced by a factor of 100 for clarity. Inset: XR data taken at room temperature. The black line is the fit to the data. b) Neutron

(nuclear and magnetic) and X-ray scattering length density (SLD) depth profiles obtained from the fits to the neutron and X-ray data, respectively. The data at $H = 186$ Oe and 335 Oe were taken successively, after applying a *negative* saturating field of $H = -5.54$ kOe. The field was applied along the $[100]$ direction.

Figure 2. (Color online) X-ray resonant magnetic scattering (XRMS) and total electron yield (TEY) XMCD spectra at the Mn absorption edge [(a) and (b)] and at the Cu absorption edge [(c) and (d)] at 30 K.

Figure 3. (Color online) X-ray magnetic reflectivity loops taken at L_3 Mn (a) and Cu (b) absorption edges at 30K applying the field along $[100]$ (red solid line) and $[110]$ (black open symbols).

Figure 4. (Color online) (a) High resolution image of a LCMO/YBCO/LCMO trilayer. EELS elemental maps using normalized integrated intensities for the O K (b), Mn $L_{2,3}$ (c), Ba $M_{4,5}$ (d) and La $M_{4,5}$ (e). The maps were produced by subtracting the background using a power law fit and then integrating the remaining intensity under the edge over windows 30 eV wide. The acquisition time was 0.03s per pixel. The color map of panel (f) has been produced by overlaying the Ba image (blue) and the Mn image (red), and the La image (green). The scale bar in all cases represents 2 nm.

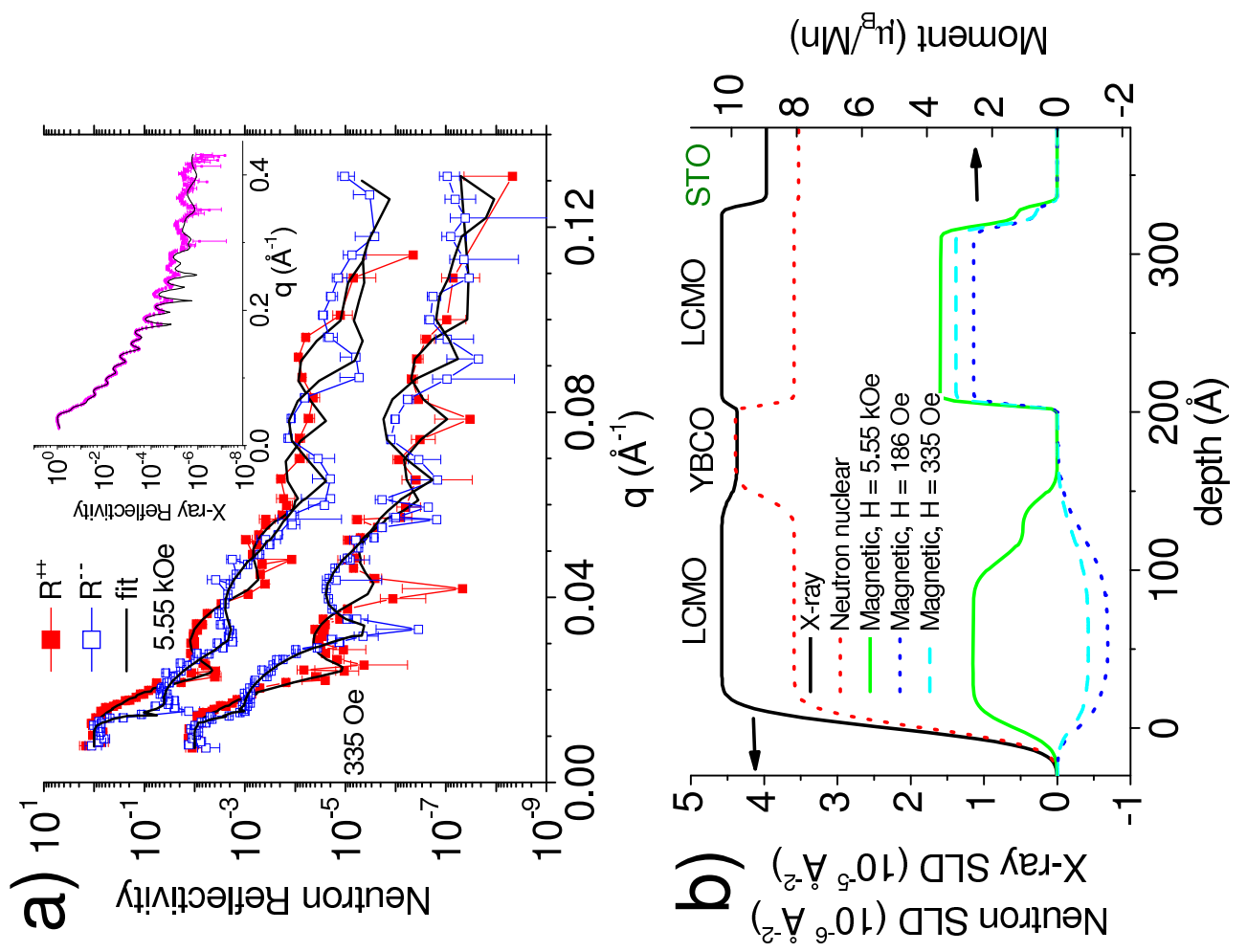


Figure 1

BCR1195

27JUL2011

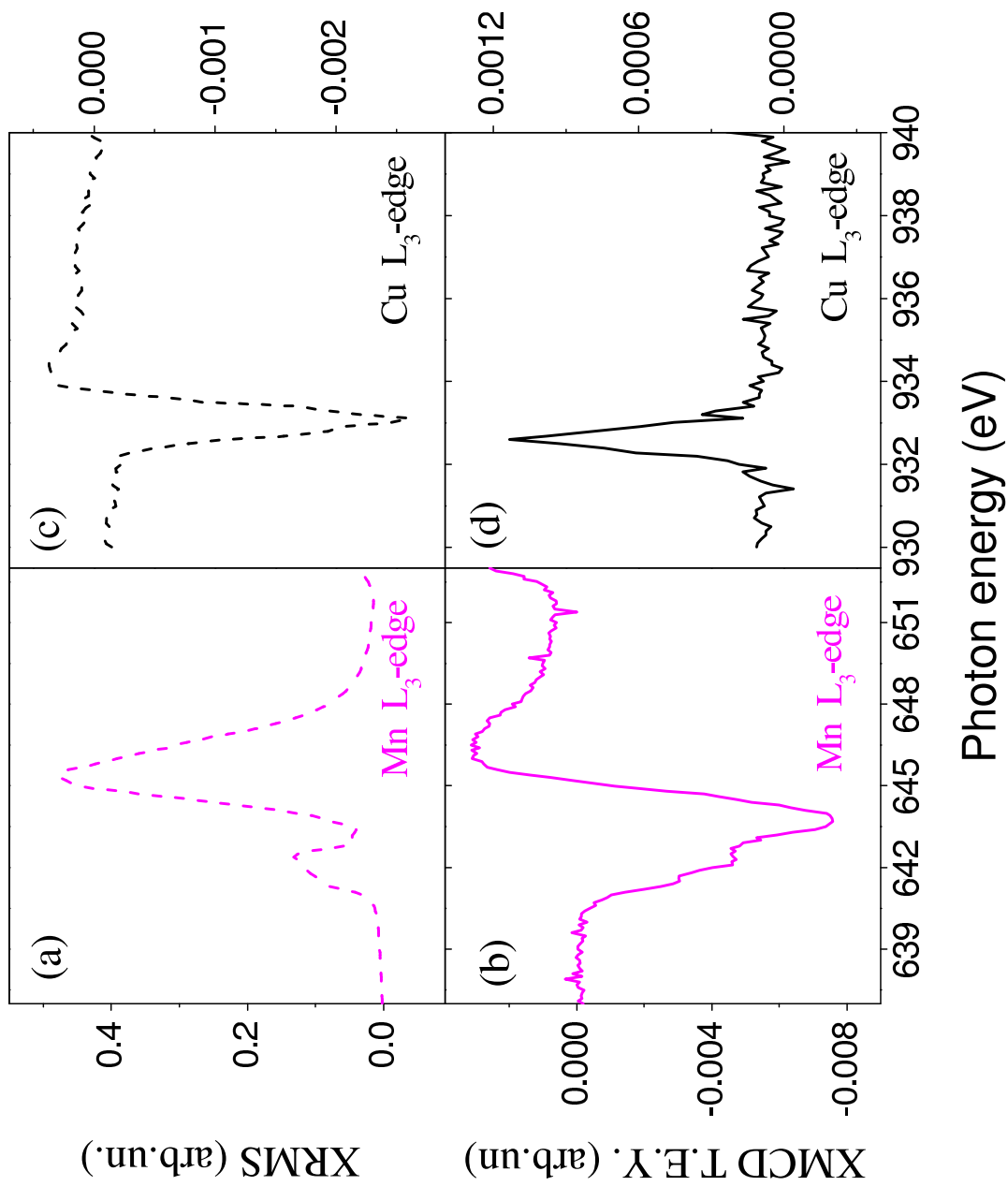


Figure 2

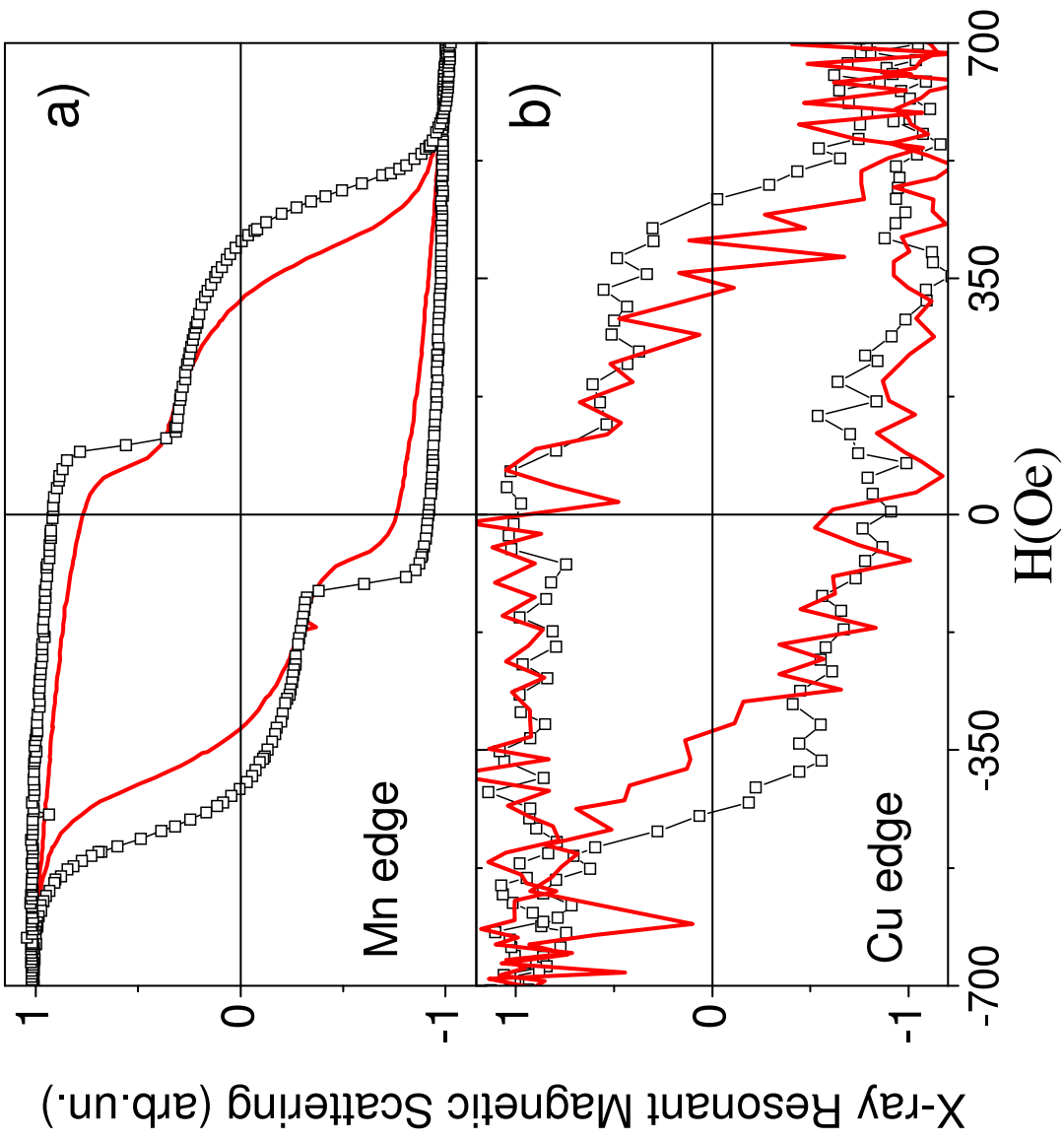


Figure 3 BCR1195 27JUL2011

Figure 3

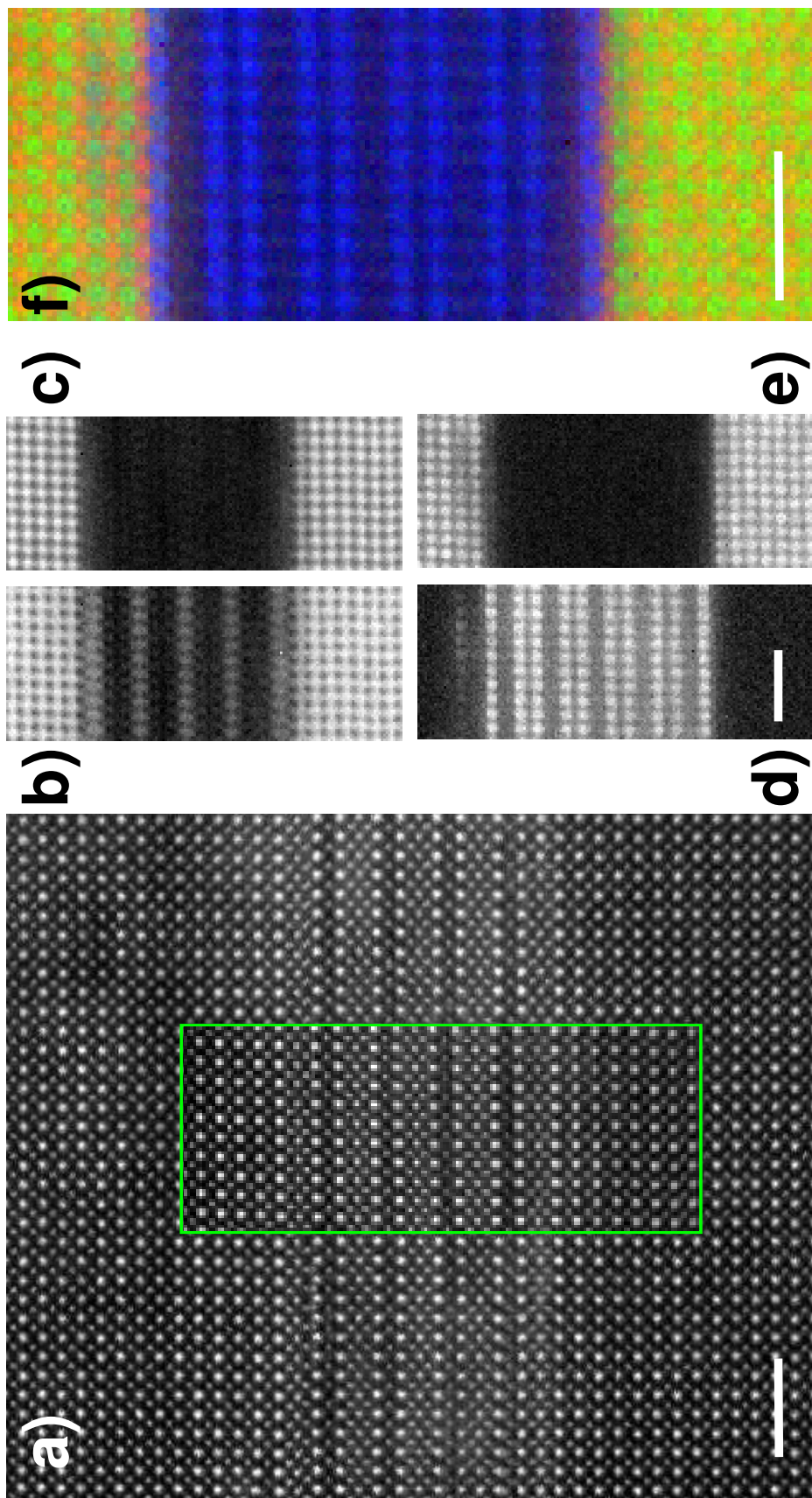


Figure 4